Structural Engineering and Mechanics, Vol. 28, No. 5 (2008) 587-601
DOI: http://dx.doi.org/10.12989/sem.2008.28.5.587

Numerical method for biaxially loaded reinforced and prestressed concrete slender columns with arbitrary section

T.J. Lou† and Y.Q. Xiang‡

Department of Civil Engineering, Zhejiang University, Hangzhou 310027, China

(Received January 24, 2006, Accepted December 28, 2007)

Abstract. In this study, a numerical procedure based on the finite element method for materially and geometrically nonlinear analysis of reinforced and prestressed concrete slender columns with arbitrary section subjected to combined biaxial bending and axial load is developed. In order to overcome the low computer efficiency of the conventional section integration method in which the reinforced concrete section is divided into a large number of small areas, an efficient section integration method is used to determine the section tangent stiffness. In this method, the arbitrary shaped cross section is divided into several concrete trapezoids according to boundary vertices, and the contribution of each trapezoid to section stiffness is determined by integrating directly the trapezoid. The space frame flexural theory is utilized to derive the element tangent stiffness matrix. The nonlinear full-range member response is traced by an updated normal plane arc-length solution method. The analytical results agree well with the experimental ones.

Keywords: slender concrete column; section integration method; finite element; arc-length algorithm; nonlinear analysis.

1. Introduction

With the quick development of modern society and economy, slender reinforced and prestressed columns are more and more frequently used to meet the requirement of people. Due to the complex material constitutive laws and the effect of secondary moments of axial force, the accurate analysis of slender concrete columns is considerably complicated. In past years, several analytical and numerical models for such columns have been developed. Some investigators (Ahmad and Weerakoon 1995, Rodriguez and Aristizabal 2001b) used analytical approaches based on the moment-curvature relationship to predict the inelastic response and failure mode of reinforced and prestressed concrete slender columns. However, the determination of the moment-curvature relationship of a column cross-section is quite difficult because the axial force, an important factor influencing the moment-curvature relationship, is a variable. Tsao and Hsu (1994) developed a numerical model for strength and deformation analysis of biaxially loaded slender columns with square and L-shaped sections, using combined finite segment and finite difference methods. Wang

† Ph.D., Corresponding author, E-mail: tjlou@zju.edu.cn
‡ Professor, E-mail: Xiangyiq@zju.edu.cn

and Hsu (1998) proposed a numerical analysis employing a B-spline function to investigate the nonlinear behavior of reinforced concrete columns. In their model, a multiplier was used for section equilibrium equation to reduce the element number. Chuang and Kong (1998) presented a numerical method for slender columns under uniaxial bending. The model was based on a simple transformation concept by transforming the concrete and steel of the critical section into an equivalent materials. Kim *et al.* (1995, 2000) outlined a plane frame element model and a space frame element model for reinforced concrete columns subjected to uniaxial bending and biaxial bending, respectively.

In conventional numerical models, the cross section of a concrete column is divided into a large number of small areas to integrate section equilibrium equations. However, this method has some limitations in application to large structures. In this paper, an efficient section model is introduced to determine the section stiffness. In this method, the arbitrary shaped cross section is divided into several concrete trapezoids according to boundary vertices, and the contribution of each trapezoid to section stiffness is determined by integrating directly the trapezoid. As a result, the element number of a concrete cross section is greatly reduced and the computational efficiency is substantially improved. On this basis, a numerical model using the space frame element theory is developed for the full-range analysis of biaxially loaded reinforced and prestressed concrete slender columns with arbitrary section.

2. Assumptions

1) Plane section remains plane after deformation.

2) Perfect bond exists between the steel and the surrounding concrete. Based on this assumption, the strain in the reinforcing steel ε_s is equal to the strain in the surrounding concrete ε_{cs}, and the strain in the prestressing steel ε_p is equal to the strain in the surrounding concrete ε_{cp} plus the initial prestrain ε_{p0}; thus

$$\varepsilon_s = \varepsilon_{cs} \tag{1a}$$

$$\varepsilon_p = \varepsilon_{cp} + \varepsilon_{p0} \tag{1b}$$

3) The stress-strain relationship for concrete in compression suggested by Hognestad (1951) is adopted in this study. It is indicated by Eqs. (2a) and (2b)

For, $\varepsilon_c \le \varepsilon_{c0}$

$$\sigma_c = f_c\left[2\frac{\varepsilon_c}{\varepsilon_{c0}} - \left(\frac{\varepsilon_c}{\varepsilon_{c0}}\right)^2\right] \tag{2a}$$

For $\varepsilon_{c0} \le \varepsilon_c \le \varepsilon_u$

$$\sigma_c = f_c\left(1 - \gamma\frac{\varepsilon_c - \varepsilon_{c0}}{\varepsilon_u - \varepsilon_{c0}}\right) \tag{2b}$$

Where σ_c = concrete stress; ε_c = concrete strain; f_c = concrete cylindrical compressive strength; ε_{c0} = concrete strain corresponding to stress f_c; ε_u = ultimate concrete compressive strain; and γ = parameter depending on the degree of confinement of the concrete.

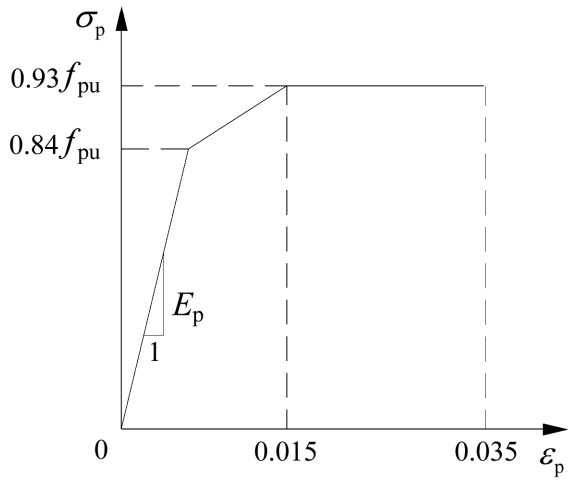

Fig. 1 Stress-strain curve of prestressing steel

4) The stress-strain relationship for concrete in tension is used as suggested by Vecchio and Collins (1986) by

For $\varepsilon_c \leq \varepsilon_{cr}$,

$$\sigma_c = E_c \varepsilon_c \tag{3a}$$

For $\varepsilon_c > \varepsilon_{cr}$,

$$\sigma_c = \frac{1}{1 + \sqrt{500\varepsilon_c}} f_t \tag{3b}$$

Where E_c = concrete elastic modulus; f_t = concrete tensile strength; and ε_{cr} = concrete cracking strain.

5) The stress-strain relationship for prestressing steel is expressed by a trilinear curve, as shown in Fig. 1, in which σ_p and ε_p = stress and strain of the prestressing steel, respectively; E_p = elastic modulus of the prestressing steel; and f_{pu} = ultimate tensile strength of the prestressing steel.

6) The stress-strain relation for reinforcing steel in both tension and compression is assumed to be elastic-perfectly plastic, as indicated by

For $\varepsilon_s \leq \varepsilon_y$,

$$\sigma_s = E_s \varepsilon_s \tag{4a}$$

For $\varepsilon_s > \varepsilon_y$,

$$\sigma_s = f_y \tag{4b}$$

Where σ_s and ε_s = stress and strain of the reinforcing steel, respectively; E_s, f_y, ε_y = elastic modulus, yield strength and yield strain of the reinforcing steel, respectively.

7) The effects of shear and torsion deformations are neglected.

3. Finite element formulations

3.1 Section tangent stiffness equation

The section model suggested by Rodriguez *et al.* (1999, 2000, 2001a), as shown in Fig. 2, is utilized in this study. The geometrical centroid o of the cross section is chosen as the origin of the section global yz-system. The section local coordinate system $o'(\xi, \eta)$ is also defined to determine the contribution of concrete to section stiffness. The ξ-axis represents the neutral axis that makes an angle α with the y-axis and produces cross points m and n with the y- and z-axes, respectively, while the η-axis is defined by the line that connects the farthest vertex e in compression with the perpendicular to the neutral axis. Two consecutive vertices i and $i+1$ define the straight line i: $\eta = a_i\xi + b_i$. The two lines drawn perpendicular from vertices i and $i+1$ to the neutral axis and the line segment i define the trapezoid i. Thus, the cross section is divided into several trapezoids according to section boundary vertices.

According to plane section hypothesis, the concrete strain ε_c at any fiber of section is given by

$$\varepsilon_c = \varepsilon_o + y\phi_z + z\phi_y \tag{5}$$

where ε_o = strain at the geometrical centroid; ϕ_y, ϕ_z = curvatures corresponding to M_y, M_z, the bending moments about the y- and z-axes, respectively.

At the place of neutral axis, $\varepsilon_c = 0$, that is

$$\varepsilon_o + y\phi_z + z\phi_y = 0 \tag{6}$$

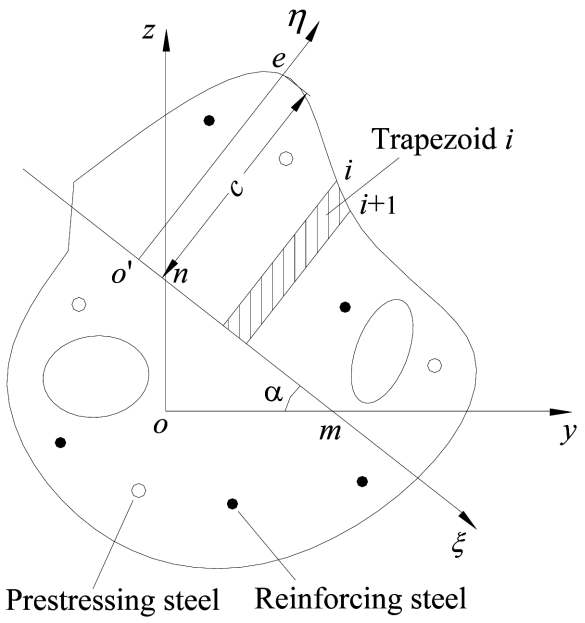

Fig. 2 Model for arbitrary prestressed concrete section

With Eq. (6), y_m, z_n are obtained as

$$y_m = -\frac{\varepsilon_o}{\phi_z}, \quad z_n = -\frac{\varepsilon_o}{\phi_y}$$

and hence

$$\tan\alpha = \frac{z_n}{y_m} = \frac{\phi_z}{\phi_y} \tag{7}$$

from Fig. 2,

$$c = |y_e \tan\alpha + z_e - z_n| \cos\alpha, \quad y_{o'} = y_e - c\sin\alpha, \quad z_{o'} = z_e - c\cos\alpha$$
$$\xi_i = (y_i - y_{o'})\cos\alpha - (z_i - z_{o'})\sin\alpha, \quad \eta_i = (z_i - z_{o'})\cos\alpha + (y_i - y_{o'})\sin\alpha$$
$$a_i = (\eta_{i+1} - \eta_i)/(\xi_{i+1} - \xi_i), \quad b_i = \eta_i - a_i\xi_i$$

where c is the distance between the farthest vertex e in compression and the origin o' of section local coordinate system.

In section local coordinate system, the concrete strain ε_c can be expressed as

$$\varepsilon_c = \frac{\phi_y}{\cos\alpha}\eta \tag{8}$$

The contribution of concrete trapezoid i to the axial force N_{ci}, the bending moment $N_{ci\xi}$ about the ξ-axis and the bending moment $N_{ci\eta}$ about the η-axis can be respectively obtained by integrating the trapezoid i as

$$N_{ci} = \int_{\xi_i}^{\xi_{i+1}} \int_0^{a_i\xi + b_i} \sigma_c \mathrm{d}\xi \mathrm{d}\eta \tag{9a}$$

$$M_{ci\xi} = \int_{\xi_i}^{\xi_{i+1}} \int_0^{a_i\xi + b_i} \sigma_c \eta \mathrm{d}\xi \mathrm{d}\eta \tag{9b}$$

$$M_{ci\eta} = \int_{\xi_i}^{\xi_{i+1}} \int_0^{a_i\xi + b_i} \sigma_c \xi \mathrm{d}\xi \mathrm{d}\eta \tag{9c}$$

Explicit forms of the integrals in Eq. (9) can be found in Rodriguez *et al.* (1999, 2001).

The equilibrium equations in the cross section for axial force N, bending moments M_y, M_z can be expressed as

$$N = \sum_{i=1}^{n_c} N_{ci} + \sum_{i=1}^{n_s} (\sigma_{si} - \sigma_{csi}) A_{si} + \sum_{i=1}^{n_p} (\sigma_{pi} - \sigma_{cpi}) A_{pi} \tag{10a}$$

$$M_y = \sin\alpha \sum_{i=1}^{n_c} M_{ci\eta} + \cos\alpha \sum_{i=1}^{n_c} M_{ci\xi} + z_{o'} \sum_{i=1}^{n_c} N_{ci} + \sum_{i=1}^{n_s} (\sigma_{si} - \sigma_{csi}) A_{si} z_{si} + \sum_{i=1}^{n_p} (\sigma_{pi} - \sigma_{cpi}) A_{pi} z_{pi} \tag{10b}$$

$$M_z = \cos\alpha \sum_{i=1}^{n_c} M_{ci\eta} + \sin\alpha \sum_{i=1}^{n_c} M_{ci\xi} + y_{o'} \sum_{i=1}^{n_c} N_{ci} + \sum_{i=1}^{n_s} (\sigma_{si} - \sigma_{csi}) A_{si} y_{si} + \sum_{i=1}^{n_p} (\sigma_{pi} - \sigma_{cpi}) A_{pi} y_{pi} \tag{10c}$$

where n_c, n_s, n_p = total numbers of the concrete trapezoids, reinforcing steel and prestressing steel, respectively; σ_{cs}, σ_{cp} = stresses in the concrete surrounding the reinforcing steel and prestressing

steel, respectively; σ_s, σ_p = stresses in the reinforcing steel and prestressing steel, respectively; and A_s, A_p = areas of the reinforcing steel and prestressing steel, respectively.

The right sides in Eqs. (10a-c) can be expressed as the functions of axial strain ε_o and curvatures ϕ_y, ϕ_z. Assuming the functions are represented by f, g and h, respectively, one has

$$N = f(\varepsilon_o, \phi_y, \phi_z) \tag{11a}$$

$$M_y = g(\varepsilon_o, \phi_y, \phi_z) \tag{11b}$$

$$M_z = h(\varepsilon_o, \phi_y, \phi_z) \tag{11c}$$

Differentiating Eq. (11) yields section tangent stiffness equation using a matrix notation as

$$d\mathbf{F} = \mathbf{D}\mathrm{d}\mathbf{C} \tag{12}$$

where

$$\mathbf{F} = [N \quad M_y \quad M_z]^T, \quad \mathbf{C} = [\varepsilon_o \quad \phi_y \quad \phi_z]^T \tag{13}$$

$$\mathbf{D} = \begin{bmatrix} \partial f/\partial \varepsilon_o & \partial f/\partial \phi_y & \partial f/\partial \phi_z \\ \partial g/\partial \varepsilon_o & \partial g/\partial \phi_y & \partial g/\partial \phi_z \\ \partial h/\partial \varepsilon_o & \partial h/\partial \phi_y & \partial h/\partial \phi_z \end{bmatrix} \tag{14}$$

3.2 Element tangent stiffness equation

A space frame element with two end nodes i and j defined in element coordinate system (x, y, z), as shown in Fig. 3, is used. Let l be the element length before deformation, and u, v and w be the x, y and z displacements of any point in the element, respectively. Assuming u is a linear function of x, and v, w are cubic functions of x, there are a total of ten coefficients that can be determined by

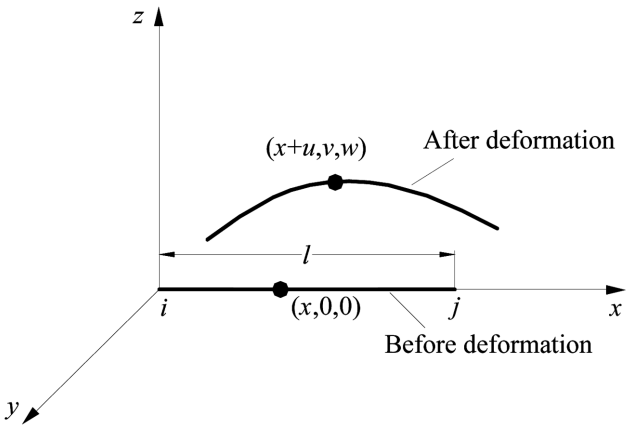

Fig. 3 Space frame element before and after deformations

element boundary condition. Then displacements u, v and w can be expressed in terms of element nodal displacements as

$$\begin{bmatrix} u \\ w \\ v \end{bmatrix} = \begin{bmatrix} \mathbf{N}_u & 0 & 0 \\ 0 & \mathbf{N}_w & 0 \\ 0 & 0 & \mathbf{N}_v \end{bmatrix} \begin{bmatrix} \mathbf{u}_{ij}^e \\ \mathbf{w}_{ij}^e \\ \mathbf{v}_{ij}^e \end{bmatrix} \tag{15}$$

where

$$\mathbf{u}_{ij}^e = [u_i \;\; u_j]^T, \quad \mathbf{v}_{ij}^e = [v_i \;\; v_i' \;\; v_j \;\; v_j']^T, \quad \mathbf{w}_{ij}^e = [w_i \;\; w_i' \;\; w_j \;\; w_j']^T \tag{16}$$

$$\mathbf{N}_u = [N_1 \;\; N_2], \quad \mathbf{N}_w = [N_3 \;\; N_4 \;\; N_5 \;\; N_6], \quad \mathbf{N}_v = [N_7 \;\; N_8 \;\; N_9 \;\; N_{10}] \tag{17}$$

$$N_1 = 1 - \frac{1}{l}x, \quad N_2 = \frac{1}{l}x, \quad N_3 = N_7 = 1 - \frac{3}{l^2}x^2 + \frac{2}{l^3}x^3$$

$$N_4 = N_8 = x - \frac{2}{l}x^2 + \frac{1}{l^2}x^3, \quad N_5 = N_9 = \frac{3}{l^2}x^2 - \frac{2}{l^3}x^3$$

$$N_6 = N_{10} = -\frac{1}{l}x^2 + \frac{1}{l^2}x^3$$

Section strains can be expressed as derivatives of displacements while the high-order derivatives is ignored

$$\mathbf{C} = [\varepsilon_o \;\; \phi_y \;\; \phi_z]^T = [u' + (v')^2/2 + (w')^2/2, w'', v'']^T \tag{18}$$

Combining Eqs. (15) and (18), the following strain-nodal displacement transition equation can be obtained

$$\mathbf{C} = (\mathbf{B}_L + \mathbf{B}_N/2)\mathbf{u}^e \tag{19}$$

where

$$\mathbf{u}^e = [\mathbf{u}_{ij}^{eT} \;\; \mathbf{w}_{ij}^{eT} \;\; \mathbf{v}_{ij}^{eT}]^T \tag{20}$$

$$\mathbf{B}_L = \begin{bmatrix} \mathbf{N}_u' & 0 & 0 \\ 0 & \mathbf{N}_w' & 0 \\ 0 & 0 & \mathbf{N}_v' \end{bmatrix}, \quad \mathbf{B}_N = [1 \;\; 0 \;\; 0]^T \mathbf{u}^{eT} (\mathbf{J}_v^T \mathbf{J}_v + \mathbf{J}_w^T \mathbf{J}_w) \tag{21}$$

$$\mathbf{J}_v = [0 \;\; 0 \;\; \mathbf{N}_v'], \quad \mathbf{J}_w = [0 \;\; \mathbf{N}_w' \;\; 0] \tag{22}$$

Variational form of Eq. (19) is

$$\delta\mathbf{C} = (\mathbf{B}_L + \mathbf{B}_N)\delta\mathbf{u}^e \tag{23}$$

Based on the virtual work principle, the following element equilibrium equation can be established

$$\delta \mathbf{u}^{eT} \mathbf{P}^e = \int_l \delta \mathbf{C}^T \mathbf{F} \mathrm{d}x \tag{24}$$

where $\mathbf{P}^e$ = element nodal load vector

Substituting Eq. (23) into Eq. (24) yields

$$\mathbf{P}^e = \int_0^l (\mathbf{B}_L + \mathbf{B}_N)^T \mathbf{F} \mathrm{d}x \tag{25}$$

Differentiating Eq. (25) gives

$$\mathrm{d}\mathbf{P}^e = \int_0^l [(\mathbf{B}_L + \mathbf{B}_N)^T \mathrm{d}\mathbf{F}] \mathrm{d}x + \int_0^l (\mathrm{d}\mathbf{B}_N^T \mathbf{F}) \mathrm{d}x \tag{26}$$

Substituting Eqs. (12) and (23) into Eq. (26) yields element tangent stiffness equation as

$$\mathrm{d}\mathbf{P}^e = \mathbf{K}^e \mathrm{d}\mathbf{u}^e = (\mathbf{K}_L^e + \mathbf{K}_N^e + \mathbf{K}_S^e) \mathrm{d}\mathbf{u}^e \tag{27}$$

where

$$\mathbf{K}_L^e = \int_0^l \mathbf{B}_L^T \mathbf{D} \mathbf{B}_L \mathrm{d}x \tag{28a}$$

$$\mathbf{K}_N^e = \int_0^l (\mathbf{B}_L^T \mathbf{D} \mathbf{B}_N + \mathbf{B}_N^T \mathbf{D} \mathbf{B}_L + \mathbf{B}_N^T \mathbf{D} \mathbf{B}_N) \mathrm{d}x \tag{28b}$$

$$\mathbf{K}_S^e = \int_0^l N (\mathbf{J}_v^T \mathbf{J}_v + \mathbf{J}_w^T \mathbf{J}_w) \mathrm{d}x \tag{28c}$$

4. Solution algorithm

4.1 Basic formulations

An updated normal plane arc-length method is adopted in this study (Lam and Morley 1992, Memon and Su 2004). As in displacement control, the arc-length solution procedure treats the load factor λ as an additional variable. Let $\mathbf{u}$ be the nodal displacement vector, and $\mathbf{P}$, $\mathbf{Q}$ be the specified nodal load and internal resisting load vectors, respectively. The out-of-balance loads $\mathbf{R}$ is given by

$$\mathbf{R} = \lambda \mathbf{P} - \mathbf{Q} \tag{29}$$

The predicted vector for the ith iteration is defined as

$$\mathbf{t}_i = (\Delta \mathbf{u}_i, \Delta \lambda_i \mathbf{P}) \tag{30}$$

in which $\Delta \lambda_i$ and $\Delta \mathbf{u}_i$ are the incremental load factor and incremental displacements, respectively, after the ith iteration.

The iterative vector between ith and $(i+1)$th iterations is defined as

$$\mathbf{n}_i = (\delta \mathbf{u}_i, \delta \lambda_i \mathbf{P}) \tag{31}$$

where

$$\delta \mathbf{u}_i = \Delta \mathbf{u}_{i+1} - \Delta \mathbf{u}_i \tag{32a}$$

$$\delta \lambda_i = \Delta \lambda_{i+1} - \Delta \lambda_i \tag{32b}$$

Let the iterative vector be normal to the predicted vector

$$\mathbf{t}_i^T \mathbf{n}_i = 0 \tag{33}$$

Substituting Eqs. (30) and (31) into Eq. (33) yields the arc-length constraint equation as

$$\Delta \mathbf{u}_i^T \delta \mathbf{u}_i + \Delta \lambda_i \delta \lambda_i \mathbf{P}^T \mathbf{P} = 0 \tag{34}$$

To keep the symmetric banded nature of the system stiffness matrix, $\delta \mathbf{u}_i$ is dismembered into two parts as

$$\delta \mathbf{u}_i = \mathbf{K}_i^{-1}(\mathbf{R}_i + \delta \lambda_i \mathbf{P}) = \delta \mathbf{u}^I + \delta \lambda_i \delta \mathbf{u}^{II} \tag{35}$$

where

$$\delta \mathbf{u}^I = \mathbf{K}_i^{-1} \mathbf{R}_i, \quad \delta \mathbf{u}^{II} = \mathbf{K}_i^{-1} \mathbf{P} \tag{36}$$

in which $\mathbf{K}_i$ is the member tangent stiffness matrix for the (i+1)th iteration; and $\mathbf{R}_i$ is the out-of-balance loads immediately after the ith iteration.

Substituting Eq. (35) into Eq. (34) gives

$$\delta \lambda_i = -\frac{\Delta \mathbf{u}_i^T \delta \mathbf{u}^I}{\Delta \mathbf{u}_i^T \delta \mathbf{u}^{II} + \Delta \lambda_i \mathbf{P}^T \mathbf{P}} \tag{37}$$

The desired incremental displacements and incremental load factor after the (i+1)th iteration can be respectively acquired by

$$\Delta \mathbf{u}_{i+1} = \Delta \mathbf{u}_i + \delta \mathbf{u}^I + \delta \lambda_i \delta \mathbf{u}^{II} \tag{38a}$$

$$\Delta \lambda_{i+1} = \Delta \lambda_i + \delta \lambda_i \tag{38b}$$

4.2 First iteration from converged point

In each arc-length increment step, the iterative procedure based on the Newton-Raphson method starting from the last converged point ($u_0, \lambda_0 \mathbf{P}$) is proceeding to eliminate the out-of-balance loads. According to geometrical relation in load-displacement space, the following equation can be obtained for the first iteration

$$\Delta \mathbf{u}_1^T \Delta \mathbf{u}_1 + \Delta \lambda_1^2 \mathbf{P}^T \mathbf{P} = \Delta L^2 \tag{39}$$

where ΔL = specified arc-length for the current increment, which is applied at the first iteration and varies at the subsequent iterations. Notice that

$$\Delta \mathbf{u}_1 = \Delta\lambda_1 \mathbf{K}_0^{-1}\mathbf{P} = \Delta\lambda_1 \mathbf{q} \tag{40}$$

where $\mathbf{K}_0$ = member tangent stiffness matrix for the first iteration, which is formed from the last converged point; and $\mathbf{q} = \mathbf{K}_0^{-1}\mathbf{P}$.

Substituting Eq. (40) into Eq. (39) gives

$$\Delta\lambda_1^2 \mathbf{q}^T\mathbf{q} + \Delta\lambda_1^2 \mathbf{P}^T\mathbf{P} = \Delta L^2 \tag{41}$$

and hence

$$\Delta\lambda_1 = \pm\sqrt{\frac{\Delta L^2}{\mathbf{q}^T\mathbf{q} + \mathbf{P}^T\mathbf{P}}} \tag{42}$$

The sign of $\Delta\lambda_1$ is chosen to enable the solution forward, and it is selected if

$$\Delta \mathbf{u}_1^T \Delta \mathbf{u}_{\mathrm{pr}} + \Delta\lambda_{\mathrm{pr}}\Delta\lambda_1 \mathbf{P}^T\mathbf{P} > 0 \tag{43}$$

where $\Delta\lambda_{\mathrm{pr}}$ and $\Delta \mathbf{u}_{\mathrm{pr}}$ are the incremental load factor and incremental displacements, respectively, of the previous increment.

5. Comparison with test results

In an experimental program by Lin and Lakhwara (1966), two slender partially prestressed concrete columns, designated as columns I and II, were tested to failure by uniaxially eccentric loading. Both columns were 3073.4 mm long, and had the same section with the same prestressing and reinforcing steel, as shown in Fig. 4. The end eccentricities of columns I and II were 76.2 mm and 50.8 mm, respectively. The material properties were as follows: E_c = 39.8 GPa, f_t = 4.0 MPa, f_c = 42.1 MPa, ε_{c0} = 0.002, ε_u = 0.0033, γ = 0.8; E_s = 200 GPa, f_y = 352 MPa; E_p = 180 GPa, f_{pu} =

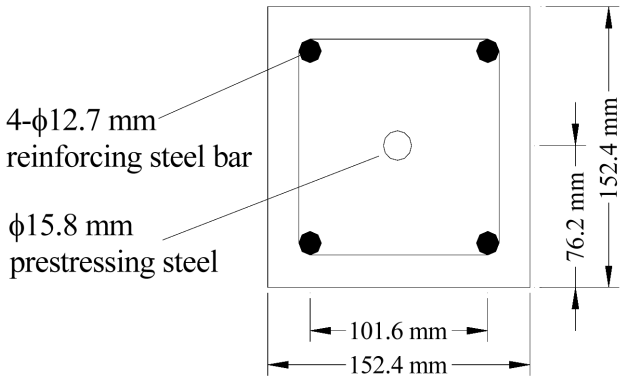

Fig. 4 Dimensions and steel details of column specimens (Lin and Lakhwara 1966)

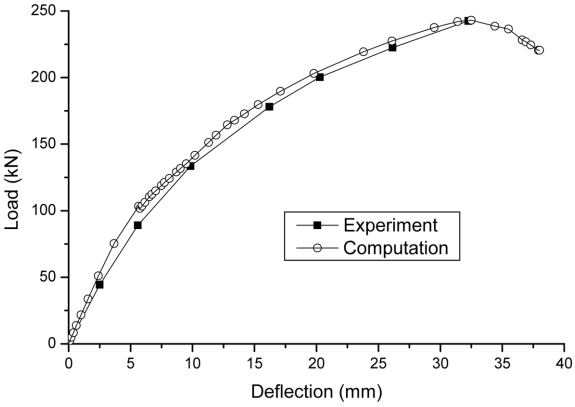

Fig. 5 Comparison of the experimental and computational load-deflection response for specimen I

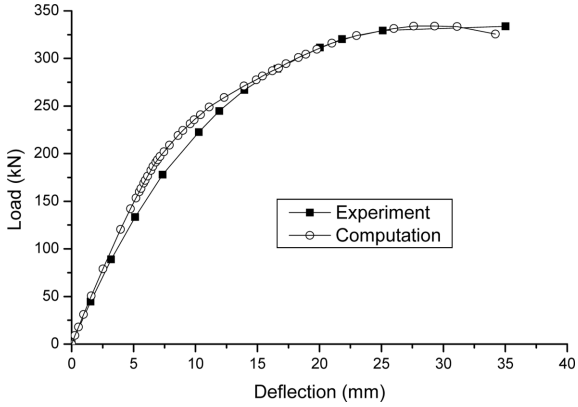

Fig. 6 Comparison of the experimental and computational load-deflection response for specimen II

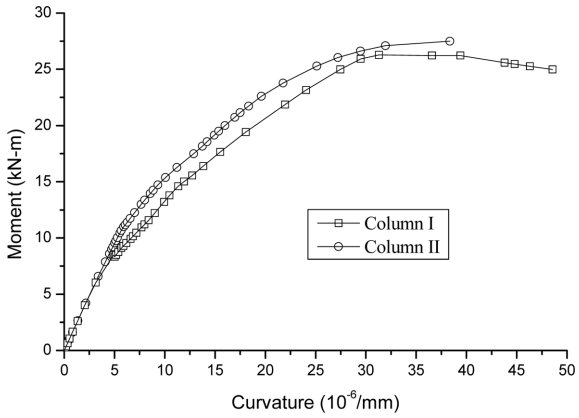

Fig. 7 Theoretical moment-curvature curves of columns I and II

1227 MPa, and effective prestress σ_{pe} = 786.6 MPa. Each column is subdivided into sixteen frame elements. The experimental and theoretical load-deflection curves for columns I and II are shown in Figs. 5 and 6, respectively. The comparisons show satisfactory agreement between the experimental and theoretical curves. The theoretical results of moment-curvature curves of the two columns are given in Fig. 7. Some numerical results (moment M, load P, midheight deflection v and curvature ϕ) on different response stages including cracking of the concrete in tension, yielding of the reinforcing steel and crushing of the concrete in compression of the column specimens are listed in Table 1.

Tsao and Hsu (1994) tested six square (C series) and eight L-shaped (B series) slender columns under combined biaxial bending and axial compression to examine the behavior of the columns. All test specimens are 1219.2 mm long and the cross sections are shown in Fig. 8. The end conditions are pin-ended. The material properties and the initial eccentricities e_y, e_z at the ends of the test columns are listed in Table 2. Assume ε_{c0} = 0.002, ε_u = 0.0045, γ = 0.45, and E_s = 200 GPa. Each test specimen is divided into sixteen space frame elements and the numerical analysis is conducted

Table 1 Numerical results on different response stages of column specimens (Lin and Lakhwara 1966)

Specimen number	Stages	M (kN-m)	P (kN)	v (mm)	ϕ (10^{-6}/mm)
I	Cracking	6.02	75.45	3.67	3.13
	Yielding	26.28	242.97	32.5	31.30
	Crushing	25.00	220.65	38.0	48.56
II	Cracking	6.59	120.50	3.94	3.38
	Yielding	26.04	334.05	27.6	27.21
	Crushing	27.50	325.60	34.2	38.35

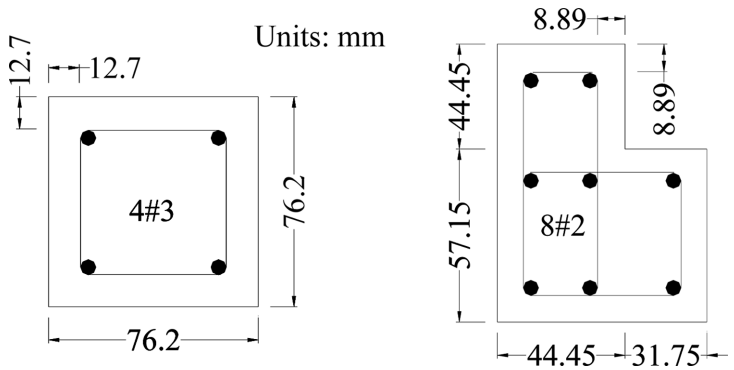

Fig. 8 Square and L-shaped specimen sections (Tsao and Hsu 1994)

Table 2 Design parameters for column specimens (Tsao and Hsu 1994)

Specimen number	f_y (MPa)	f_c (MPa)	f_t (MPa)	E_c (GPa)	e_y (mm)	e_z (mm)
B2	434.39	25.07	2.13	32.0	21.46	46.05
B3	434.39	26.79	2.28	32.5	26.95	26.95
B4	434.39	26.79	2.28	32.5	35.92	35.92
B5	441.28	29.35	2.49	33.5	8.99	8.99
B6	441.28	29.35	2.49	33.5	17.96	17.96
B7	441.28	29.21	2.48	33.5	15.47	20.14
B8	441.28	29.21	2.48	33.5	30.94	40.31
C1	503.33	19.11	1.62	29.5	9.73	23.47
C2	503.33	18.58	1.58	29.0	17.96	17.96
C3	503.33	29.04	2.47	33.5	35.92	35.92
C4	420.6	25.51	2.17	32.2	17.96	17.96
C5	420.6	25.51	2.17	32.2	19.43	46.94
C6	420.6	25.51	2.17	32.2	9.73	23.47

using the proposed numerical model. The comparisons of the experimental and computational maximum loads P_{max} and corresponding midheight deflections v and w for seven L-shaped and six

square specimens are given in Table 3. The maximum loads and corresponding midheight deflections predicted by the proposed method show a good agreement with the experimental data. Figs. 9-11 show the comparisons of the experimental load-deflection curves and the computational predictions for specimens B2, C4 and C5, respectively. It can be seen in Figs. 9-11 that the proposed numerical procedure well reproduces the response of the test specimens throughout their elastic, inelastic and failure load ranges.

Table 3 Comparisons of the experimental and computational results for column specimens (Tsao and Hsu 1994)

Specimen number	P_{max} (kN)			v (mm)			w (mm)		
	Test	Analysis	Error (%)	Test	Analysis	Error (%)	Test	Analysis	Error (%)
B2	44.68	44.21	−1.05	17.5	14.5	−17.14	10.2	9.8	−3.92
B3	55.89	54.68	−2.17	18.3	16.3	−10.93	7.1	7.8	9.86
B4	44.10	45.06	2.18	20.8	18.1	−12.98	9.7	8.3	−14.43
B5	124.35	114.75	−7.72	9.4	10.1	7.44	5.1	5.5	7.84
B6	70.06	72.23	3.10	15.5	13.9	−10.32	7.1	6.4	−9.86
B7	70.02	73.47	4.93	12.2	11.2	−8.20	6.9	7.1	2.90
B8	45.86	45.07	−1.72	16.5	15.2	−7.88	11.7	9.6	−17.95
C1	67.66	66.59	−1.58	6.1	7.1	16.39	17.3	16.2	−6.36
C2	55.89	58.73	5.08	11.9	12.8	7.56	12.4	12.8	3.22
C3	39.19	42.73	9.03	13.2	14.0	6.06	14.2	14.0	−1.41
C4	82.92	80.22	−3.26	9.7	9.0	−7.22	10.2	9.0	−11.77
C5	46.68	46.22	−0.99	9.7	9.0	−7.22	16.3	13.2	−19.02
C6	81.40	77.45	−4.85	7.6	7.1	−6.58	14.0	12.6	−10.00

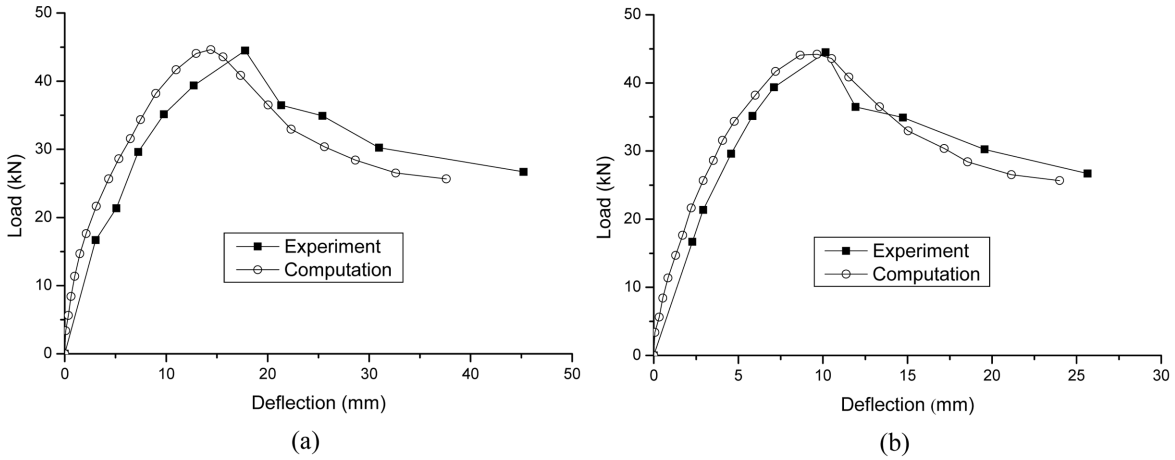

Fig. 9 Comparison of the experimental and computational load-deflection response for specimen B2. (a) y direction, (b) z direction

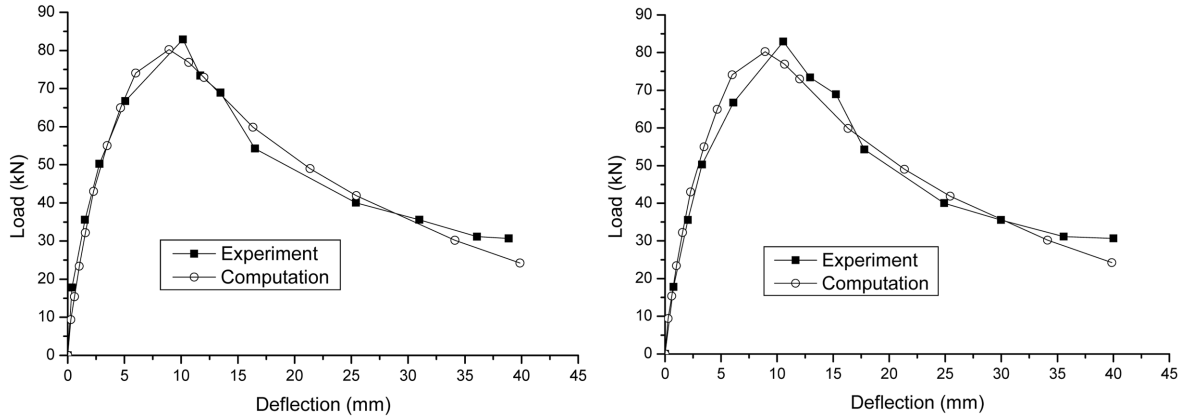

Fig. 10 Comparison of the experimental and computational load-deflection response for specimen C4. (a) y direction, (b) z direction

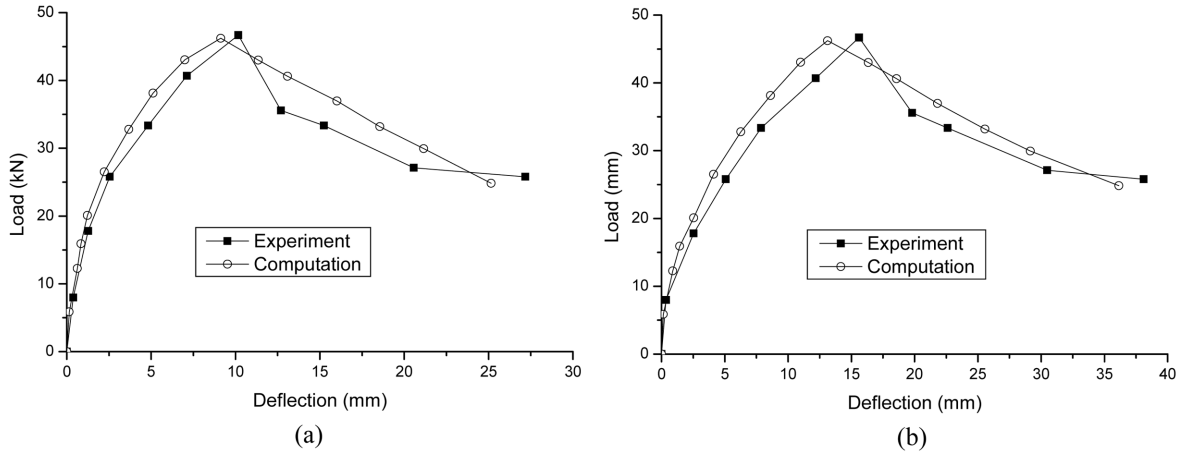

Fig. 11 Comparison of the experimental and computational load-deflection response for specimen C5. (a) y direction, (b) z direction

6. Conclusions

A finite element model for nonlinear full-range analysis of reinforced and prestressed concrete slender columns with arbitrary section subjected to combined biaxial bending and axial compression is developed. Both material and geometrical nonlinearities are taken into consideration. With nonlinear stress-strain relationship for concrete, prestressing and reinforcing steel, an excellent section model was introduced to determine the section tangent stiffness matrix by directly integrating the trapezoids divided from the concrete section according to boundary vertices. The nonlinear space frame element is used to derive the element tangent stiffness matrix that can be partitioned into three sub-matrices reflecting three different nonlinear effects. An updated normal plane arc-length method is incorporated into the finite element procedure to trace the full-range

response of the columns. Some test columns are analyzed and the accuracy and effectiveness of the proposed procedure is verified.

References

Ahmad, S.H. and Weerakoon, S.L. (1995), "Model for behavior of slender reinforced concrete columns under biaxial bending", *ACI Struct. J.*, **92**(2), 188-198.

Chuang, P.H. and Kong, S.K. (1998), "Strength of reinforced concrete columns", *J. Struct. Eng.*, ASCE, **124**(9), 992-998.

Hognestad, E. (1951), "A study of combined bending and axial load in reinforced concrete members", Bulletin No. 399, University of Illinois Engineering Experiment Station, Urbana, IL, USA.

Kim, J.K. and Yang, J.K. (1995), "Buckling behaviour of slender high-strength concrete columns", *Eng. Struct.*, **17**(1), 39-51.

Kim, J.K. and Lee, S.S. (2000), "The behavior of reinforced concrete columns subjected to biaxial bending", *Eng. Struct.*, **22**(11), 1518-1528.

Lam, W.F. and Morley, C.T. (1992), "Arc-length method for passing limit points in structural calculation", *J. Struct. Eng.*, **118**(1), 169-185.

Lin, T.Y. and Lakhwara, T.R. (1966), "Ultimate strength of eccentrically loaded partially prestressed columns", *PCI J.*, **11**(3), 37-49.

Memon, B.A. and Su, X.Z. (2004), "Arc-length technique for nonlinear element analysis", *J. Zhejiang University: Science*, **5**(5), 618-628.

Rodriguez, J.A. and Aristizabal, J.D. (1999), "Biaxial interaction diagrams for short RC columns of any cross section", *J. Struct. Eng.*, ASCE, **125**(6), 672-683.

Rodriguez, J.A. and Aristizabal, J.D. (2000), "Partially and fully prestressed concrete sections under biaxial bending and axial load", *ACI Struct. J.*, **97**(4), 553-563.

Rodriguez, J.A. and Aristizabal, J.D. (2001a), "*M-P-*ϕ diagrams for reinforced, partially, and fully prestressed concrete sections under biaxial bending and axial load", *J. Struct. Eng.*, ASCE, **127**(7), 763-773.

Rodriguez, J.A. and Aristizabal, J.D. (2001b), "Reinforced, partially, and fully prestressed slender concrete columns under biaxial bending and axial load", *J. Struct. Eng.*, ASCE, **127**(7), 774-783.

Tsao, W.H. and Hsu, C.T.T. (1994), "Behaviour of biaxially loaded square and L-shaped slender reinforced concrete columns", *Mag. Concrete Res.*, **46**(169), 257-267.

Vecchio, F.J. and Collins, M.P. (1986), "The modified compression field theory for reinforced concrete elements subjected to shear", *ACI Struct. J.*, **83**(2), 219-231.

Wang, G.G. and Hsu, C.T.T. (1998), "Nonlinear analysis of reinforced concrete columns by cubic-spline function", *J. Eng. Mech.*, ASCE, **127**(4), 803-810.